

Article

Determination of Field of View of a Dawn–Dusk Sun-Synchronous Orbit Satellite Based on Improved Observation Mode

Dandan Xie ^{1,2}, Yawei Huang ^{1,*}  and Changxiang Yan ¹

¹ Changchun Institute of Optics, Fine Mechanics and Physics, Chinese Academy of Sciences, Changchun 130033, China; xiedandan@ciomp.ac.cn (D.X.); yancx0128@126.com (C.Y.)

² University of Chinese Academy of Sciences, Beijing 100049, China

* Correspondence: huangyawei@ciomp.ac.cn

Abstract: We report a method for determining the field of view (FOV) of a dawn–dusk sun-synchronous orbit satellite based on an improved observation mode. The target trajectory distribution model in geosynchronous orbit (GEO) is established, the natural rendezvous mode is improved, and the observation mode of the satellite is determined. A scheme for determining the thresholds of cross-orbit field of view (COFOV) and the along-orbit field of view (AOFOV) was developed. The result shows that the coverage of the satellite can reach more than 95% when the improved observation mode is used to observe the GEO target. When the revisit period of the satellite is one day, the threshold of the COFOV is 15°, and the threshold of the AOFOV is 12°.

Keywords: dawn and dusk sun-synchronous orbit satellite; cross-orbit field of view; along-orbit field of view; observation mode; geostationary Earth orbit belt



Citation: Xie, D.; Huang, Y.; Yan, C. Determination of Field of View of a Dawn–Dusk Sun-Synchronous Orbit Satellite Based on Improved Observation Mode. *Appl. Sci.* **2022**, *12*, 7475. <https://doi.org/10.3390/app12157475>

Received: 28 June 2022

Accepted: 21 July 2022

Published: 26 July 2022

Publisher's Note: MDPI stays neutral with regard to jurisdictional claims in published maps and institutional affiliations.



Copyright: © 2022 by the authors. Licensee MDPI, Basel, Switzerland. This article is an open access article distributed under the terms and conditions of the Creative Commons Attribution (CC BY) license (<https://creativecommons.org/licenses/by/4.0/>).

1. Introduction

Because geosynchronous orbit (GEO) satellites have the advantages of low propellant consumption required for operation, continuous signal coverage for fixed areas, and easy alignment with ground communication antennas, many countries have frequently deployed artificial satellites in GEO in recent years. The GEO space targets have become increasingly congested, and space target collisions have occurred on occasion. The debris created by the collisions poses a hazard to the space targets' safety. To avoid satellite collisions, it is critical to identify, locate, monitor, and categorize space targets [1,2]. In order to achieve this goal, researchers have proposed the Space-Based Space Surveillance (SBSS) plan. This system has two significant advantages: one is the dynamic perception of space targets. The purpose of monitoring space objects is achieved by identifying, locating, and cataloguing space objects. The other is early warning. When space debris or abandoned aircraft threaten to collide with aircraft in normal operation, an early warning can be given in advance, and the threat can be avoided by controlling the aircraft to change the orbit altitude.

The SBSS program was originally developed by the United States [3,4]. The Midcourse Space Experiment (MSX) satellite, launched in 1996, was the first space-based surveillance satellite deployed by the United States. The satellite is in a sun-synchronous orbit (SSO) at an altitude of 800 km, and it is equipped with a space-based visible (SBV) sensor with a $6.4^\circ \times 1.6^\circ$ field of view (FOV), which considerably enhances the sensor's revisit rate to critical targets and the capacity to detect and monitor artificial satellites [5,6]. Following the successful test of the MSX satellite, the US launched the SBSS project in 2002, with the goal of improving real-time perception of the space warfare environment and establishing a space surveillance network (SSN). The first SBSS satellite, Block 10, was launched into a 630 km sun-synchronous low Earth orbit (LEO) in 2010 and began operations in 2013. The satellite was primarily used to monitor targets in geostationary Earth orbit (GEO)

and can meet both measurement accuracy and wide-area search capability performance requirements [7]. Flohrer and colleagues presented a strategy for space-based surveillance of space objects, particularly GEO targets, in 2011. The aim was to launch a satellite into an SSO with an orbital altitude of 800 km, with a sensor with a field of view of $6^\circ \times 6^\circ$. This spacecraft can cover all controlled GEO satellites in one day, but it takes 1.5 to 3 days to cover uncontrolled GEO satellites and space debris [8]. Sapphire, Canada's first military satellite, was successfully launched in 2013. The satellite operates in a dawn–dusk sun-synchronous orbit (DDSSO) at an altitude of 786 km. The satellite contains a payload with an FOV of $1.4^\circ \times 1.4^\circ$ that is primarily used to identify medium- and high-orbit space debris from low orbit, and it will eventually join the US SSN. In 2013, Canada launched the NEOSS satellite at the same time. The optical system has an FOV of $0.85^\circ \times 0.85^\circ$ and an aperture of 15 cm [9].

Researchers at the Lincoln Laboratory in the United States have also pushed for more research into the space-based observation method of observing GEO targets from LEO satellites [1,10]. They originally presented a GEO belt-based pinch point (PP) area observation mode, which uses the LEO satellite's narrow FOV sensor to scan a tiny region of the GEO belt and achieves high detection effectiveness for most GEO objects [11]. Following that, Utzmann et al. presented an observation mode of the Earth's shadow edge, which can accomplish the observation goal by controlling the sensor on the DDSSO satellite to always point to a certain area of the Earth's shadow edge [12]. The European Space Agency (ESA) proposed a "leak-proof fence" architecture for viewing GEO targets in 2014 [13]. This mode "intercepts" the GEO belt by commanding the observation sensor to set up a fence with an FOV across a 30° orbit on the GEO belt, allowing for the observation of more than 85 percent of the GEO objects in a single day [13]. Hu et al. presented a new pseudo-fixed latitude observation mode in 2017 based on the GEO belt development rule. In this mode, the sensor's orientation is dynamically modified based on the GEO band's sinusoidal distribution, allowing most GEO targets to be viewed with a limited FOV [14]. The summarized research status shows that when satellite detection needs are specified, the orbital features and observation tactics of the satellite have a direct impact on the sensor's FOV.

For space-based visual sensors, there are commonly two observing modalities. The first is the natural rendezvous observation mode, in which the sensor is typically fixed on the observation satellite and passively monitors the GEO target using only the features of the satellite's own orbital motion. The other option is active observation, in which the sensor's orientation is modified using various tactics to cover certain spatial regions. The pseudo-fixed latitude observation mode is a novel, natural intersection mode [14], and the natural rendezvous observation mode is a frequently utilized observation mode for space-based surveillance systems. Because LEO satellites have a small orbital radius, they may scan the GEO band numerous times a day [15]. DDSSO is the low orbit with a short orbital period. In this orbit, satellites can run multiple laps in one day and visit GEO targets multiple times to achieve higher observation efficiency. At the same time, the satellite runs on the DDSSO and can maintain good optical observation conditions throughout the day. Because of their orbital features, DDSSO satellites offer favorable optical observation conditions for most of the year [16]. As a result, the observation satellites specified in this study are LEO satellites in DDSSO that naturally rendezvous with the GEO target in the pseudo-fixed latitude observation mode. There are four common approaches for getting the satellite to view the chosen GEO targets in a short amount of time:

- (a) An observation constellation is made up of many satellites carrying separate sensors.
- (b) Building an observation fence to cover the whole GEO belt using active observation mode.
- (c) Multiple sensors with different orientations are carried by a single satellite.
- (d) A sensor with a large enough FOV is carried by a single satellite.

From a purely engineering standpoint, using a single satellite to perform an observation plan is easier than using numerous satellites, and carrying a single sensor on the

same satellite is easier than carrying multiple sensors of the same sort at the same time. Furthermore, the approach of erecting the observation fence is no longer appropriate due to the evolution of the PP zone of the GEO belt. As a result, the most typical observation strategy is to carry a single big FOV sensor on a single satellite. The implementation of this observation method is complicated by the need to achieve a broad FOV. However, as image sensor production technology improves, the area array of the image sensor grows, and the FOV that can be reached by a single sensor grows. Furthermore, related researchers presented a multi-scale FOV splicing technology to overcome the problem of big FOV observations being difficult to perform, assessed the practicality of this technology through tests, and applied it to an actual space-based detection system [17,18]. The higher the FOV, the better the observation effectiveness of the space-based detecting system, but the more difficult the image sensor manufacturing process becomes. Simultaneously, it mandates the employment of more image sensors for splicing, increasing the cost and difficulty of system development significantly. As a result, selecting an appropriate FOV for space-based detection systems is essential.

At present, there are roughly two methods for determining the FOV of the space-based observation system. Method 1: Assume the space target to be a Poisson distribution, and use the spherical formula and statistical star table to determine the FOV [19]. Method 2: Assume the spatial target as a Gaussian distribution, and use the probability distribution model to determine the FOV [20]. This article examines the plan wherein the DDSSO satellite observes the GEO targets. First, we identified the categories of GEO targets, analyzed the orbital evolution law of the failed satellites and other space debris, established the evolution model, and obtained the trajectory distribution characteristics of all targets in the GEO belt. In addition, an improved observation model based on the natural rendezvous model was developed. After that, a scheme for determining the cross-orbit field of view (COFOV) and the along-orbit field of view (AOFOV) was formulated, and the correctness of the conclusion was verified by simulation experiments. Finally, the threshold FOV that meets the requirements of both coverage rate and revisit period was obtained, and the corresponding orbital altitude and inclination of the satellite were determined. The traditional FOV determination methods were all studied with the detection probability as the index. Compared with the traditional method, the FOV determination method in this paper not only considers the detection probability, but also considers the observation plan, the revisit period, and the satellite orbit and inclination. The research in this paper is more comprehensive and more universal.

2. Determination of the Satellite Observation Mode

According to whether the sensor pointing is controlled with the operation of the satellite, the observation mode of the satellite can be divided into two categories:

(a) The passive observation mode (the natural rendezvous mode).

In the passive observation mode, the observation satellite does not need to control the pointing of the sensor, which is usually fixed on the satellite and only relies on the characteristics of its own orbital motion to passively observe the GEO target. The Sapphire Project in Canada, the surveillance satellite constellation built by Lockheed Martin Space Systems in the United States, and the SBO telescope photographed by ESA scientists all adopt this observation mode.

(b) The active observation mode.

In the active observation mode, the pointing of the satellite sensor is adjusted through different strategies in order to cover certain space areas. The PP area gaze observation mode proposed by the Lincoln Laboratory adopts the active observation mode.

In order to choose an observation mode suitable for the satellite studied in this paper, we first divided GEO targets into three categories: the valid satellites, the failed satellites, and other space debris. Among them, the valid satellites can maintain a 0° inclination angle through continuous orbital maneuvers, while the failed satellites and other space debris

undergo periodic evolution under the influence of perturbation forces. Next, we analyzed the evolution of the failed satellites and other space debris.

In inertial space, the orbital plane normal vector expressed as I determines the position and orientation of the orbit plane (see Figure 1a).

$$I = \begin{bmatrix} i_x \\ i_y \\ i_z \end{bmatrix} = \begin{bmatrix} \sin i \sin \Omega \\ -\sin i \cos \Omega \\ \cos i \end{bmatrix}, \tag{1}$$

where i is expressed as the orbital inclination, and Ω is expressed as the right ascension of the ascending node (RAAN). Under the combined influence of the Earth’s oblateness, the zonal sector, and the lunisolar gravitation, the orbital inclination vector of the GEO celestial bodies will drift clockwise around the pole at coordinate $(0, -7.4^\circ)$ within a period of 54 years [21]. The circular curve in Figure 1b represents the approximate relationship between the RAAN and the orbital inclination of the invalid GEO target at any time.

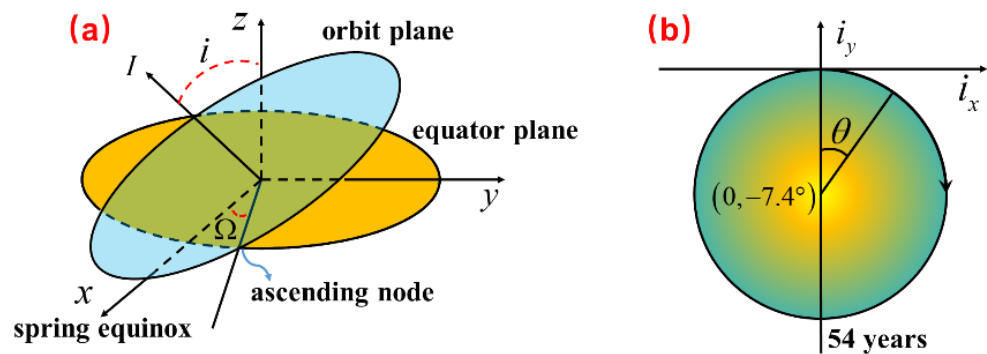


Figure 1. (a) Orbital plane with orbital inclination; (b) Evolution Law of Orbital Inclination.

In the Earth-centered inertial (ECI), the target’s right ascension α and declination δ are generally used to represent the target’s trajectory. Since $\sin i > 0$, and Ω of GEO objects beyond control are in the region of $\Omega \in (-90^\circ, 90^\circ)$, the result leads to [21].

$$\sin i = 2B \cos \Omega \tag{2}$$

In addition, through the relationship between i , Ω , α , and δ , the extreme condition of δ is deduced. The result shows that the δ of GEO targets are always between envelopes δ_{\max} and δ_{\min} [21].

$$\begin{cases} \delta_{\max} = \sin^{-1}[B(\sin \alpha + 1)] = B/(\sin \alpha + 1) \\ \delta_{\min} = \sin^{-1}[B(\sin \alpha - 1)] = B/(\sin \alpha - 1) \end{cases} \tag{3}$$

Let B be equal to 7.4° [14,21], then the value range of B/ can be obtained from Equation (3) as $(7.4^\circ, 7.5^\circ)$. Considering the limitation of the value range of α , and in order to make the envelope interval cover most of the GEO targets, the B is set to be approximately 7.5° [21]. Figure 2a shows the relationship between i and Ω . Figure 2b shows the theoretical distribution of GEO objects beyond control. Therefore, the trajectories of GEO targets can be surrounded by envelopes δ_{\max} and δ_{\min} . The trajectories of the GEO target present a band-like distribution of sine equal width, and the δ span of the GEO band at any α is approximately 15° .

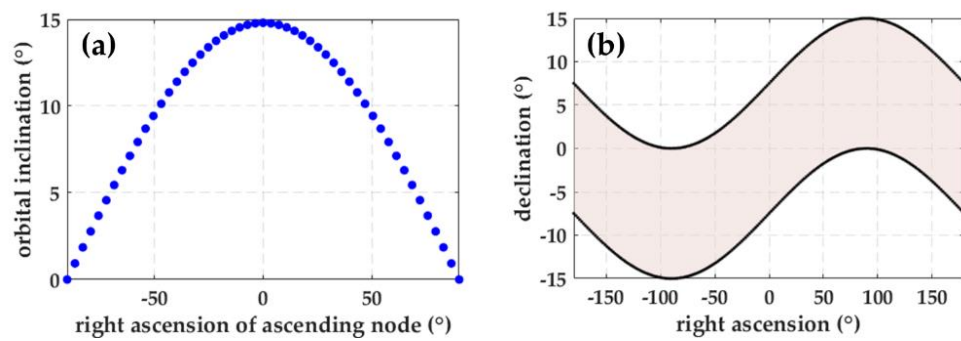


Figure 2. (a) The relationship between RAAN and inclination. (b) Theoretical distribution of GEO objects beyond control.

According to the sinusoidal distribution characteristics of GEO targets, in order to make the observation satellite effectively cover the GEO belt, we improved the passive observation mode [21]. This observation mode is based on the passive observation mode, with the vernal equinox, summer solstice, autumnal equinox, and winter solstice as time nodes, and the pointing of the satellite sensor is adjusted periodically. When the satellite observes the target, the latitude pointed at by the sensor remains the same throughout the day. According to the changing characteristics of the GEO belt, the sensor’s pointing is finely adjusted once per day. Compared with the traditional passive observation mode, this observation mode is more effective for the observation of the GEO belt. And due to the influence of the moment generated on the GEO target orbital surface by the gravity of the sun and the moon and the perturbation of the Earth’s oblateness, the PP area gradually becomes inconspicuous. Compared with the PP area observation mode in the active observation mode, this observation mode not only makes it easier to adjust the pointing of the camera, but also can observe the entire GEO belt. Since the observation satellite runs in a DDSSO, the celestial coordinate system with the Earth’s center as the origin has two characteristics (see Figure 3). One is long-term characteristics. The orbital surface processes one circle a year, and the coordinate axis also moves with the year as a cycle. Another is short-term characteristics. Due to the small precession angle of the SSO in the short term, the coordinate system can be regarded as an inertial coordinate system. By analyzing the observation characteristics of the satellite, we obtain the pointing trajectory equation of the sensor on the celestial sphere [21].

$$(x + \varphi)^2 + [z - (\gamma + \delta)]^2 = R^2, \tag{4}$$

where γ is expressed as the pitch angle, and φ is expressed as the yaw angle. At the same time, the position of the sensor pointing to deep space should also consider the inclination limit of the orbit. The inclination of an SSO is defined as i , and the δ of the orbital center is $i - 90^\circ$. When the passive observation mode is used to observe the GEO belt, the observation area is a circle with the coordinate $(-\varphi, \gamma + \delta)$ as the center and R as the radius [21]. The size of the observation area is fixed, but the location is variable. When the latitude of the observation area is fixed, there is a “seasonal decline problem” in the observation as the GEO distribution changes. To solve this problem, we improved the passive observation mode. Under this observation mode, the orientation of the sensor is adjusted with the change of the GEO target distribution, and the center of the observation area is controlled to the center of the GEO zone corresponding to the observation moment. Therefore, the GEO belt can be well covered in the daily observation area throughout the year.

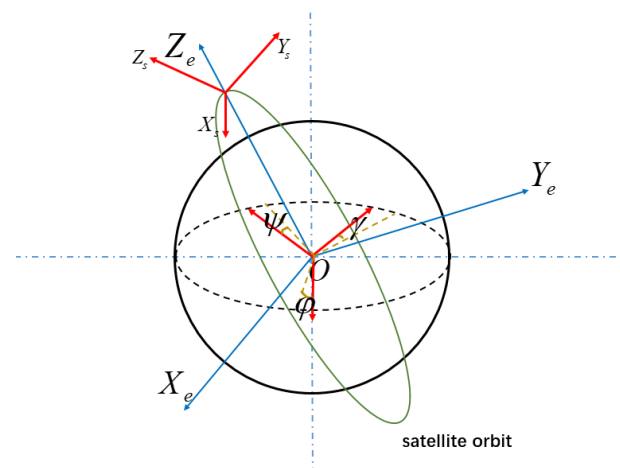


Figure 3. The celestial coordinate system with the center of the Earth as the origin.

Figure 4 shows the trajectories of all GEO targets on 21 March 2021, Beijing time. Comparing the changes in the observation area before and after the improvement, we conclude that by improving the satellite observation model, an observation model that is more suitable for the current GEO target distribution can be obtained. In this observation mode, we can control the selection of the FOV while ensuring the coverage of the satellite.

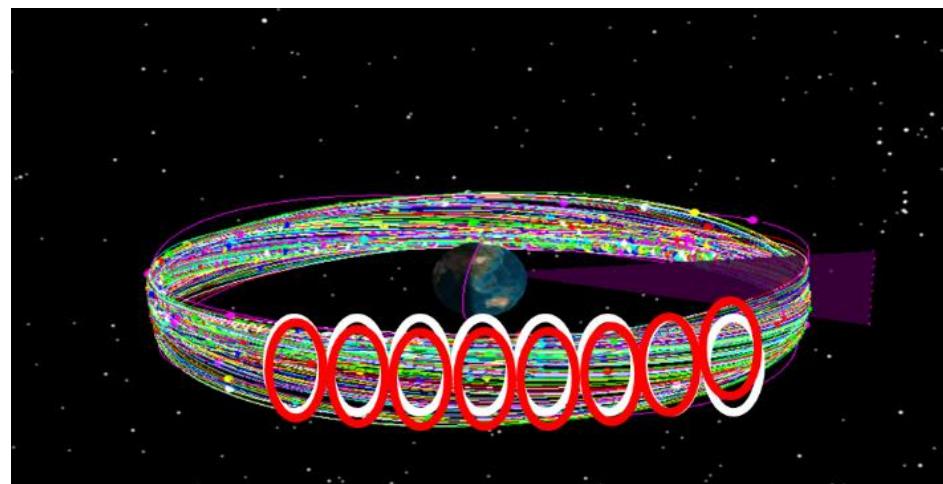


Figure 4. The pointing area of the satellite's sensor. (The white area in the figure represents the observation area before the improved observation mode is used, and the red area in the figure represents the observation area after the improved observation mode is used.)

3. Threshold FOV of the Satellite Based on the Improved Observation Mode

In order to describe the determined field of view more conveniently, we divided the FOV into the cross-orbit field of view (COFOV) and the along-orbit field of view (AOFOV) and determined their thresholds respectively. An important factor in determining whether a GEO target can be observed is whether the target can enter the FOV of the sensor. The size of sensor's FOV in turn determines the coverage range of the GEO belt by the observation satellite. In summary, when a satellite operating in a DDSSO observes the GEO belt under the improved observation mode, in order to meet the sensor coverage requirements, the sensor's COFOV must be greater than 15° . In order to verify the correctness of the above theoretical derivation, we simulated the coverage rate of sensors in different FOVs. First, we set the COFOV to 15° and kept it unchanged, and simulated the changes of the sensor coverage with the observation days when the AOFOV ranged from 4° to 8° . The simulation results are shown in Figure 5.

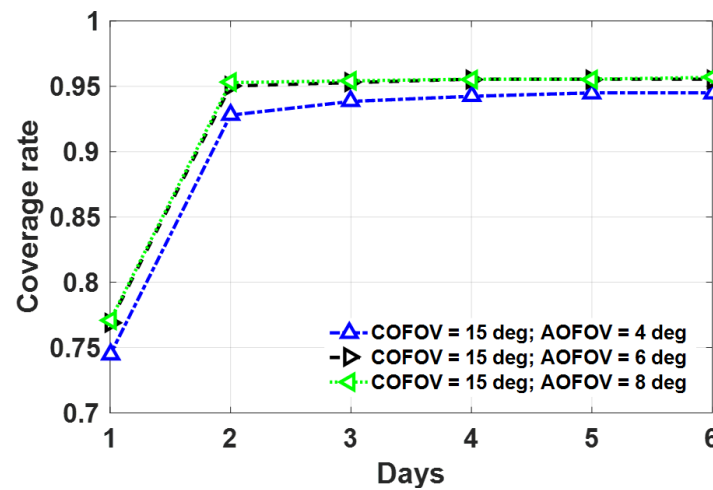


Figure 5. Sensor coverage rate with cross-orbit FOV value of 15° and along-orbit FOV value from 4° to 8°.

Figure 5 shows that the coverage rate of the observation satellite is less affected by the sensor’s AOFOV, and the coverage rate difference under different AOFOVs hardly changes with the observation days. When the COFOV is fixed, the coverage rate does not change after the AOFOV reaches a certain value. When the AOFOV reaches 6°, the coverage rate reaches a maximum value. Next, we set the sensor’s AOFOV to 4° and changed the COFOV from 13° to 20°, simulating the coverage rate of the observed satellite (see Figure 6).

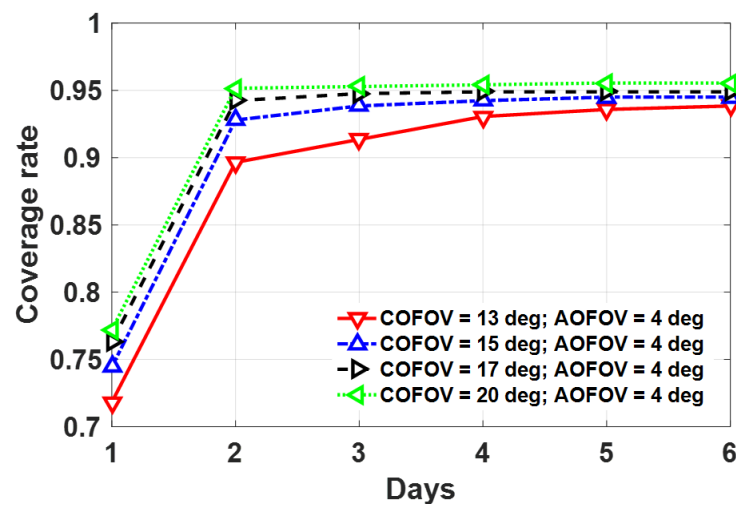


Figure 6. Sensor coverage rate with cross-orbit FOV value from 13° to 20° and along-orbit FOV value of 4°.

Figure 6 shows that with the increase in the COFOV, the coverage rate will increase, but the growth rate shows a gradually decreasing trend. The threshold COFOV is 15°. When the COFOV is smaller than the threshold COFOV, the coverage rate increases rapidly. When the COFOV is larger than the threshold COFOV, the coverage rate increases slowly. According to the above simulation analysis, compared with the AOFOV, the COFOV is the main factor affecting the satellite coverage rate. Under the specific conditions of observing the GEO belt by a DDSSO satellite, it is reasonable to select the sensor’s COFOV to be 15°.

Based on the characteristics of satellite observation patterns, we determined the threshold COFOV, and according to the simulation results, we determined that the coverage rate of the satellite can be guaranteed under this threshold, which proves the rationality of the COFOV threshold. Next, we focused on determining the threshold for AOFOV.

Although the AOFOV of the sensor has little effect on the coverage rate of the observation satellite, it will directly affect the scanning width of the satellite to the GEO belt, which in turn affects the revisit period of the satellite to the GEO belt. Therefore, the AOFOV of the sensor needs to be constrained to meet the revisit period requirements of the observation satellite. Next, we used the relevant theory of orbit design to constrain the AOFOV of the spaceborne sensor.

From the analysis in the previous section, the observation area formed by the sensor in the natural rendezvous mode is circular. Assuming that the GEO band is narrow, the GEO band can be viewed as a rectangle in the short term. Therefore, the width of the sensor sweep across the GEO strip in one cycle is only related to the sensor's AOFOV. Due to the small FOV, it is difficult for the sensor to scan such a wide range of GEO bands in one orbital period. If we ensure that the sensor can revisit the GEO target within a few days, we must ensure that the GEO strip areas scanned by the sensor each day do not completely overlap, and we must ensure that the observing satellites do not operate an integer number of turns per day. Otherwise, in natural rendezvous mode, the observation sensor would see the same batch of targets every day.

$$N = \frac{T_g}{T}, \quad (5)$$

where N is expressed as daily laps of the observation satellite, T_g is expressed as the rotation period of the Earth, and T is expressed as the orbital period of the observation satellite. The orbital period can be represented by the orbital altitude of the observing satellite.

$$T = 2\pi\sqrt{\frac{(R_e + h)^3}{\mu}}, \quad (6)$$

where R_e is the average radius of the Earth, h is the orbit altitude, and μ is the Earth's gravitational constant. Assuming that the observation satellite can complete the revisit of the GEO target within P days, the following conditions must be met:

$$\frac{360\text{deg}}{2\text{AOFOV}} = P \times N, \quad (7)$$

Since N cannot be an integer, we define the following representation of N :

$$N = K + m/M, \quad (8)$$

where K is the integer part of N , and m/M is the fractional part of N . Furthermore, m is a key parameter that determines the order of scanning bands on the GEO belt with the value range of $1, 2 \dots M - 1$, and m and M are relatively primes. The satellite can circle the Earth $KM + m$ times in M days, resulting in an integer number of scanning bands. Therefore, M is called the revisit period of the GEO belt. Condition: $(KM + m)D \geq 360\text{deg}$ needs to be met if the satellite is to revisit the GEO band. Where D is the scanning width of the GEO belt by the observation satellite in each orbital period, and its value is twice AOFOV. The minimum revisit period of the observation satellite is expressed as M_{\min} .

$$M_{\min} = \left\lceil \frac{360\text{deg}}{KD} - \frac{m}{K} \right\rceil + 1, \quad (9)$$

According to Equations (5) and (6), the corresponding relationship between the number of laps per day and the orbit height of the observation satellite is shown in Table 1.

Table 1. Correspondence between daily laps and orbital altitude of satellites.

| Daily Laps | 13 | 14 | 15 | 16 |
|-----------------------|---------|--------|--------|--------|
| orbital altitude (km) | 1262.09 | 893.79 | 566.89 | 274.42 |

The altitude constraint for a DDSSO is [580 km, 1200 km], and the period constraint is [96.27 min, 109.42 min]. According to Table 1, we can obtain the value range of N as (13, 15), and according to Equation (8), we can obtain the value of K as 13 and 14. Then, we can obtain the orbital inclination from the constraint of the observed satellite.

$$\sigma = \arccos \left[-0.09885657 / \left(\frac{R_E}{R_E + h} \right)^{3.5} \right], \tag{10}$$

The integer part of the daily operation circle of the observation satellite is determined, that is, $K = 14$. The corresponding relationship between the revisit period of the observation satellite and the sensor’s scanning width can be summarized (see Table 2).

Table 2. Correspondence between the revisit period and the minimum scanning width under different M and m .

| Revisit Period: 1 Day | | | | | | |
|------------------------|---|------------|------------|-----------|---|---|
| Minimum Scanning Width | | m | | | | |
| | | 1 | 2 | 3 | 4 | 5 |
| M | 1 | * | * | * | * | * |
| | 2 | 24.000 deg | * | * | * | * |
| | 3 | 24.000 deg | * | * | * | * |
| | 4 | 24.000 deg | * | * | * | * |
| | 5 | 24.000 deg | * | * | * | * |
| | 6 | 24.000 deg | * | * | * | * |
| Revisit Period: 2 Days | | | | | | |
| Minimum Scanning Width | | m | | | | |
| | | 1 | 2 | 3 | 4 | 5 |
| M | 1 | * | * | * | * | * |
| | 2 | * | * | * | * | * |
| | 3 | 12.414 deg | 12.000 deg | * | * | * |
| | 4 | 12.414 deg | * | * | * | * |
| | 5 | 12.414 deg | 12.000 deg | * | * | * |
| | 6 | 12.414 deg | * | * | * | * |
| Revisit Period: 3 Days | | | | | | |
| Minimum Scanning Width | | m | | | | |
| | | 1 | 2 | 3 | 4 | 5 |
| M | 1 | * | * | * | * | * |
| | 2 | * | * | * | * | * |
| | 3 | * | 8.182 deg | * | * | * |
| | 4 | 8.372 deg | * | 8.000 deg | * | * |
| | 5 | 8.372 deg | 8.182 deg | 8.000 deg | * | * |
| | 6 | 8.372 deg | * | * | * | * |

Table 2. *Cont.*

| | | Revisit Period: 4 Days | | | | |
|------------------------|---|------------------------|-----------|-----------|-----------|-----------|
| Minimum Scanning Width | | <i>m</i> | | | | |
| | | 1 | 2 | 3 | 4 | 5 |
| M | 1 | * | * | * | * | * |
| | 2 | * | * | * | * | * |
| | 3 | * | * | * | * | * |
| | 4 | * | * | * | * | * |
| | 5 | 6.316 deg | 6.207 deg | 6.102 deg | 6.000 deg | * |
| | 6 | 6.316 deg | * | * | * | * |
| | | Revisit Period: 5 Days | | | | |
| Minimum Scanning Width | | <i>m</i> | | | | |
| | | 1 | 2 | 3 | 4 | 5 |
| M | 1 | * | * | * | * | * |
| | 2 | * | * | * | * | * |
| | 3 | * | * | * | * | * |
| | 4 | * | * | * | * | * |
| | 5 | * | * | * | * | * |
| | 6 | 5.070 deg | * | * | * | 5.800 deg |

* means non-existent.

According to Equations (5)–(10) and Table 2, we have sorted out the relationship between the revisit period and the sensor’s AOFOV, the number of daily laps of the satellite, and the altitude and inclination of the satellite’s orbit (see Table 3).

Table 3. The relationship between the revisit period, the along-orbit FOV, the daily laps, the orbit altitude, and the orbit inclination.

| Revisit Period | AOFOV _{min} (deg) | Daily Laps | Orbit Altitude (km) | Orbit Inclination (deg) |
|----------------|----------------------------|------------|---------------------|-------------------------|
| 1 day | 12.000° | 14 + 1/2 | 725.6459 | 98.2876 |
| | | 14 + 1/3 | 780.6078 | 98.5156 |
| | | 14 + 1/4 | 808.4900 | 98.6334 |
| | | 14 + 1/5 | 825.3501 | 98.7051 |
| | | 14 + 1/6 | 836.6453 | 98.7533 |
| 2 days | 6.207° | 14 + 1/3 | 780.6078 | 98.5156 |
| | | 14 + 1/4 | 808.4900 | 98.6334 |
| | | 14 + 1/5 | 825.3501 | 98.7051 |
| | | 14 + 1/6 | 836.6453 | 98.7533 |
| | 6.000° | 14 + 2/3 | 671.7269 | 98.0680 |
| | | 14 + 2/5 | 758.4958 | 98.4235 |
| 3 days | 4.186° | 14 + 1/4 | 808.4900 | 98.6334 |
| | | 14 + 1/5 | 825.3501 | 98.7051 |
| | | 14 + 1/6 | 836.6453 | 98.7533 |
| | 4.091° | 14 + 2/3 | 671.7269 | 98.0680 |
| | | 14 + 2/5 | 758.4958 | 98.4235 |
| | 4.000° | 14 + 3/4 | 645.1487 | 97.9614 |
| | | 14 + 3/5 | 693.1714 | 98.1549 |
| 4 days | 3.158° | 14 + 1/5 | 825.3501 | 98.7051 |
| | | 14 + 1/6 | 836.6453 | 98.7533 |
| | 3.104° | 14 + 2/5 | 758.4958 | 98.4235 |
| | | 14 + 3/5 | 693.1714 | 98.1549 |
| 5 days | 3.000° | 14 + 4/5 | 629.3215 | 97.8984 |
| | | 14 + 1/6 | 836.6453 | 98.7533 |
| | 2.900° | 14 + 5/6 | 618.8195 | 97.8568 |

The satellite revisit period and the number of laps per day determine the minimum AOFOV of the sensor. The altitude and inclination of the satellite’s orbit depend on the number of laps the satellite operates per day. Under the improved observation mode, the

sensor’s COFOV is set to 15° . Corresponding to the orbital altitude and inclination of the satellite, the AOFOV of the sensor is set to the minimum value in each case. The simulation results for all the cases in Table 3 are shown in Figure 7.

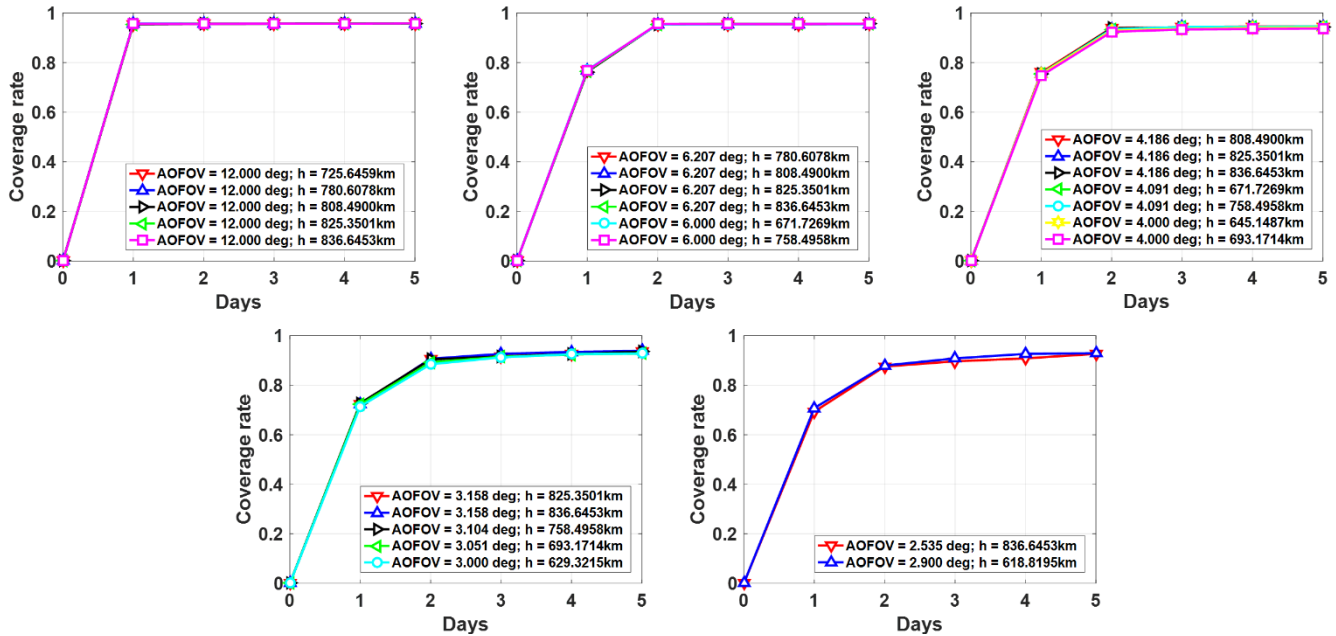


Figure 7. Simulation results of the minimum FOV in the along-orbit direction that meets the requirements when the revisit period of the satellite ranges from 1 day to 5 days.

The simulation results in Figure 7 intuitively verify our theoretical derivation. When the AOFOV is 12° , it only takes one day to revisit the GEO target to be observed. When the AOFOV is 6° , it takes two days to revisit the GEO target to be observed. When the AOFOV is 4° , it takes three days to revisit the GEO target to be observed. When the AOFOV is 3° , it takes four days to revisit the GEO target to be observed. As the AOFOV gradually decreased, the number of revisit days required increased. When the revisit period is fixed, changes in satellite orbital altitude and inclination due to the different daily laps will not affect the satellite coverage.

4. Conclusions

FOV is one of the important performance indicators of space-based detection systems. The selection of the FOV should not only ensure the indicator requirements of the coverage rate and the revisit period of the satellite, but also consider the existing technical conditions. Therefore, it is very important to choose a reasonable sensor FOV. Based on the observation strategy and orbit characteristics of satellites, we studied the detection FOV of the DSSO satellites used to observe GEO targets, and verified the correctness of the theoretical derivation through simulation experiments. The innovations of the research results of this paper are as follows:

- (a) By analyzing the evolution law of the GEO targets, we obtained the characteristics that the trajectory of the GEO target presents a band-like distribution of sine equal width. We improved the passive observation mode and proposed an observation mode suitable for observing the distribution characteristics of the current GEO target trajectory.
- (b) In the improved observation mode, the sensor’s field of view was divided into COFOV and AOFOV, and their thresholds were determined respectively. On the premise that the coverage rate of the observation satellite to the GEO target reaches 95%, when the revisit period of the satellite is one day, the threshold of COFOV is 15° , and the

threshold of AOFOV is 12° ; when the revisit period of the satellite is two days, the threshold of COFOV is 15° , and the threshold of AOFOV is 6° . Additionally, according to the orbit theory, the orbital height and inclination angle of the satellite in two cases are determined respectively.

For the space-based space target detection system, given the clear system detection requirements, the method in this paper can provide the threshold FOV of the sensor that meets the detection index. We provided some constructive guidance for the selection of the FOV of the detection system, and the method for determining the FOV can be more widely applicable to the space-based space target detection system, providing a reference for their FOV selection.

Author Contributions: Conceptualization: D.X.; methodology: D.X. and Y.H.; software: D.X. and Y.H.; validation: C.Y.; formal analysis: D.X.; investigation: D.X. and Y.H.; resources: D.X.; writing—original draft preparation: D.X.; writing—review and editing: Y.H. All authors have read and agreed to the published version of the manuscript.

Funding: This research was funded by the National Natural Science Foundation of China (NSFC), grant number 62105331.

Conflicts of Interest: The authors declare no conflict of interest.

References

- Losacco, M.; Schirru, L. Orbit Determination of Resident Space Objects Using the P-Band Mono-Beam Receiver of the Sardinia Radio Telescope. *Appl. Sci.* **2019**, *9*, 4092. [[CrossRef](#)]
- Schirru, L.; Pisanu, T.; Podda, A. The Ad Hoc Back-End of the BIRALET Radar to Measure Slant-Range and Doppler Shift of Resident Space Objects. *Electronics* **2021**, *10*, 577. [[CrossRef](#)]
- Gaposchkin, E.M.; Braun, C.; Sharma, J. Space-Based Space Surveillance with the Space-Based Visible. *J. Guid. Control. Dyn.* **2000**, *23*, 148–152. [[CrossRef](#)]
- Burnham, W.F.; Morton, F.E., Jr.; Sridharan, R.; Viggh, H.E.; Wiseman, A.J.; Zollinger, G.R. Mission Planning for Space-Based Surveillance with the Space-Based Visible Sensor. *J. Guid. Control. Dyn.* **2000**, *23*, 165–169. [[CrossRef](#)]
- Stokes, G.H.; Braun, C.; Sridharan, R.; Sharma, J. The space-based visible program. *Linc. Laboratory J.* **1998**, *11*, 205–229.
- Sharma, J. Space-Based Visible Space Surveillance Performance. *J. Guid. Control. Dyn.* **2000**, *23*, 153–158. [[CrossRef](#)]
- Sharma, J.; Stokes, G.H.; Braun, C.; Zollinger, G.; Wiseman, A.J. Toward Operational Space-Based Space Surveillance. *Linc. Laboratory J.* **2002**, *13*, 309–334.
- Flohrer, T.; Krag, H.; Klinkrad, H.; Schildknecht, T. Feasibility of performing space surveillance tasks with a proposed space-based optical architecture. *Adv. Space Res.* **2011**, *47*, 1029–1042. [[CrossRef](#)]
- Maskell, P.; Oram, P. Sapphire: Canada's answer to space-based surveillance of orbital objects. In Proceedings of the Advanced Maui Optical and Space Surveillance Technologies Conference, Maui, HI, USA, 16–19 September 2008.
- Wang, X.Y.; An, W.; Wu, Y.H.; Li, J. Research on Space-based Optical Surveillance's Observation Strategy of Geostationary-Orbit's Pitch Point Region. In Proceedings of the Conferences of the Photoelectronic Technology Committee of the Chinese Society of Astronautics, Beijing, China, 13–15 May 2014.
- Wang, X.Y.; An, W.; Wu, Y.H.; Li, J. Research on space-based optical surveillance's observation strategy of geostationary-orbit's pitch point region. *Proc. SPIE Int. Soc. Opt. Eng.* **2015**, *9521*, 403–408.
- Utzmann, J.; Wagner, A. Space-Based Space Surveillance as Complementary Element in an SSA Architecture. In Proceedings of the European Space Surveillance Conference, Madrid, Spain, 7–9 June 2011.
- Silha, J.; Schildknecht, T.; Hinze, A.; Utzmann, J.; Wagner, A.; Willemsen, P.; Teston, F.; Flohrer, T. Capability of Space-Based Space Surveillance System to Detect and Track Objects in GEO, MEO and LEO Orbits. In Proceedings of the 65th International Astronautical Congress, Toronto, ON, Canada, 29 September–3 October 2014. IAC-14-A6.1.1.
- Hu, Y.P.; Chen, L.; Huang, J.Y. Space-based Pseudo-fixed Latitude Observation Mode Based on the Characteristics of Geosynchronous Orbit Belt. *Acta Astronaut.* **2017**, *137*, 31–37. [[CrossRef](#)]
- Luo, J.; Chen, L.; Tang, G.J. Attitude optimization of optical space surveillance satellite to observe specific geostationary orbit object. *Optik Z. für Licht- und Elektronenoptik: = J. Light-Electron Optic* **2016**, *127*, 11706–11716. [[CrossRef](#)]
- Huafei, D.; Zhi, L. The Research on the Pointing Strategy of Space-based Visible Space Surveillance. *Aerosp. Control* **2011**, *29*, 39–43.
- Brady, D.J.; Gehm, M.E.; Stack, R.A.; Marks, D.L.; Kittle, D.S.; Golish, D.R.; Vera, E.M.; Feller, S.D. Multiscale gigapixel photography. *Nature* **2012**, *486*, 386–389. [[CrossRef](#)] [[PubMed](#)]
- Stamenov, I.; Arianpour, A.; Olivas, S.J.; Agurok, I.P.; Johnson, A.R.; Stack, R.A.; Morrison, R.L.; Ford, J.E. Panoramic monocentric imaging using fiber-coupled focal planes. *Opt. Express* **2014**, *22*, 31708. [[CrossRef](#)] [[PubMed](#)]

19. Chunqiu, X. *The Study on Off-Axis Optical System with Wide Field of View for Space-Based Detection Camera*; Changchun Institute of Optics, Fine Mechanics and Physics, Chinese Academy of Sciences: Changchun, China, 2017.
20. Dang, H.; Yu, H.; Deng, L.; Jiang, G. Modeling and Simulation of Detection Probability for Whole Airspace Oriented Optical Target. *J. Syst. Simul.* **2015**, *27*, 1214–1220.
21. Hu, Y.P.; Li, K.B.; Xu, W.; Chen, L.; Huang, J.Y. A novel space-based observation strategy for GEO objects based on daily pointing adjustment of multi-sensors. *Adv. Space Res.* **2016**, *58*, 505–513. [[CrossRef](#)]